Journal of Materials Chemistry C

RSC Publishing

PAPER

View Article Online
View Journal | View Issue

Synthesis of low-temperature-processable and highly conductive Ag ink by a simple ligand modification: the role of adsorption energy

Cite this: *J. Mater. Chem. C*, 2013, **1**, 1855

Inyu Jung, Kihyun Shin, Na Rae Kim and Hyuck Mo Lee*

Acetic acid (AA) has been employed to reduce the surface capping ligands of Ag nanoparticles (NPs) for the fabrication of low-temperature-processable and highly conductive Ag ink. The ligand reduction of the Ag NPs was achieved using a one-step method, in which oleylamine (OA)-capped Ag NPs were immersed in AA for different durations (1, 2, 3, 5 and 10 h). The weight of the total capping ligand was reduced from 12.1 wt% to 2.3 wt% by 10 h AA immersion. According to *in situ* transmission electron microscopy (TEM) and electrical resistivity, the ligand-reduced Ag NPs were cured at a much lower temperature (approximately 100 °C) and showed better electrical performance than OA-capped NPs under the same conditions. To investigate the reason for this enhancement of the electrical properties, we characterized the surface chemistry of the Ag NPs by Fourier transform infrared spectroscopy (FTIR) and X-ray photoelectron spectroscopy (XPS), which revealed that the surface capping ligand was exchanged from the OA to the acetate ion. In addition, the adsorption energy of the ligand was increased by the ligand exchange, which was studied using density functional theory (DFT) calculations. DFT was effective in explaining the adsorption of each ligand on Ag NPs and indicated that the ligand can be exchanged by AA immersion.

Received 19th October 2012
Accepted 2nd January 2013

DOI: 10.1039/c2tc00450j

www.rsc.org/MaterialsC

Introduction

Traditionally, vacuum deposition and photolithography have presented the disadvantages of multiple steps, high processing temperature, and high cost, as well as the production of toxic waste. Printed electronics have recently become an attractive alternative to the conventional patterning technique because the new processes are fast, simple and inexpensive and even provide processability at low temperatures.[1–4] The drivers of the current printed electronics market are organic photovoltaic devices,[5,6] flexible batteries,[7–9] electro-optic devices,[10,11] flexible displays,[12] thin film transistors,[13,14] sensor arrays[15] and radio frequency identification tags.[16] All of these devices require electrical contact and conductive structures, and metals are the main system because of their superior conductivity, although several candidates have been studied as conductive materials, including molten metals, conductive polymers and a metallic nanoparticle (NP) suspension.[17–19] Ink made of metal NPs and an appropriate solvent can be used at room temperature and has better direct current conductivity (typically 10^4 to 10^5 S cm^{-1}) than conductive polymers (typically 10 to 10^2 S cm^{-1}).[20] However, the curing process is still conducted near 250 °C,[21] which is not compatible with plastic substrates, such as polyethylene terephthalate or polycarbonate, which have relatively low glass transition temperatures (T_g). Therefore, low-temperature-processable and highly conductive ink is necessary for use with plastic substrates.

Capping ligand modification (reduction, addition and exchange) presents promising opportunities and challenges because the capping ligand is fully covered on the NPs during chemical synthesis. Ligand modification is a well-known method for tuning the surface properties of NPs that involves adding an excess of ligand to the NP solution, which results in the displacement of the original ligand from the NP surface. In particular, ligand exchange reactions on noble metal NPs through the self-assembly of thiols have been studied for many years.[22,23] Most ligands discussed in the previous reports contain a carboxylate ion (COO^-)[24–26] or an alcohol (OH)[27] endgroup that is chemically adsorbed to the surface of the NPs and forms a stable ligand layer. Recently, several groups have reported the percolation transformation and noted the relationship between the curing temperature and the loss of ligand shells.[20,28,29] Although the capping ligand is necessary for the chemical synthesis of NPs, it is not required for electrical contact or conductive patterns. Based on these requirements, the reduction of the capping ligand has also been studied in an effort to improve the electrical properties over the last few years.[30,31]

However, it is difficult to analyze ligand modification experimentally because it is too small to observe, and it is difficult to capture the moment of ligand modification. Using density functional theory (DFT) calculations, we can manipulate

Department of Materials Science and Engineering, KAIST, 291 Daehak-Ro, Yusung-Gu, Daejeon, Republic of Korea 305-701. E-mail: hmlee@kaist.ac.kr; Fax: +82-42-350-3310; Tel: +82-42-350-3334

atoms one by one, compare the adsorption energy of various ligands, and predict the reaction pathway of the ligand modification. In practice, many researchers use DFT calculations to investigate adsorption energy and structural stability and to provide helpful explanations of experimental results.[32–37]

To the best of our knowledge, there has been no previous report on the enhancement of electrical properties by a simple ligand modification. In this study, we achieved ligand exchange and ligand reduction using an acetic acid (AA) immersion treatment. The enhancement of the electrical properties was analyzed by a four-point probe station and *in situ* transmission electron microscopy (TEM), and the ligand exchange was characterized by Fourier transform infrared spectroscopy (FTIR) and X-ray photoelectron spectroscopy (XPS) analyses of the NP surface. In addition, we used the DFT calculation of adsorption energy for a theoretical study of ligand exchange.

Experimental

Materials and evaluation

The mono-dispersed Ag NPs were prepared following the procedure reported in our previous study.[30] Briefly, 2.5 g of silver nitrate ($AgNO_3$, Sigma-Aldrich) was added to 100 mL of oleylamine (OA, $C_{18}H_{37}N$, Sigma-Aldrich) while being stirred. Next, OA-capped Ag NPs with a diameter of 12.2 nm ($\sigma \leq 7.7\%$) were synthesized at 180 °C (high-temperature ripening stage) for 1 h and then at 150 °C (low-temperature incubation stage) for 5 h. The product was purified using a dispersion–centrifugation process several times, and an additional methanol (CH_3OH, Sigma-Aldrich) dipping treatment was conducted to reduce the additional surface-capping OA.[31,38,39] The Ag NPs were then immersed in 99.9% acetic acid (CH_3COOH, Sigma-Aldrich) for different time periods (1, 2, 3, 5 and 10 h) to reduce the OA from the Ag NPs.[40,41] After the AA immersion treatment, ethanol (C_2H_5OH, Sigma-Aldrich) was poured into the suspension, which was then centrifuged at 10 000 rpm for 30 min. The resulting NPs were dispersed again with ethanol in a homogenizer bath (Sonic Dismembrator) and centrifuged again. Finally, 30 wt% Ag NP was dispersed in ethanol-based solvents to fabricate the conductive ink. To measure the decrease in the residual surface ligand, we employed a thermogravimetry analyzer (TGA).[30,42] The temperature was increased from 50 °C to 1000 °C at a heating rate of 20 °C min^{-1}. To investigate the agglomeration of Ag NPs with different ligands and increasing temperature from 25 °C to 300 °C, we used *in situ* TEM operated at 300 kV.[43] The curing process was conducted after spin-coating at temperatures of 100 °C, 150 °C, 200 °C and 250 °C for different durations, and the sheet resistance was measured using a four-point probe station. Moreover, field emission scanning electron microscopy (FE-SEM) was employed to analyze the surface morphology and the vertical section of the conductive films.

Characterization of ligand exchange

FTIR and XPS analyses were conducted to characterize the ligand. To collect the FTIR spectra of the ligand-capped Ag NPs, samples were dried at 30 °C in a vacuum oven prior to pellet fabrication. KBr (300 mg) was mixed and crushed with 3 mg of Ag NPs, and 200 mg of the mixture was used for pellet fabrication.[25] Each FTIR spectrum was recorded between 4000 and 500 cm^{-1}. For the FTIR spectra of the OA and AA solvent, we used an attenuated total reflectance FTIR cell. In addition, OA-capped and ligand-reduced NPs were placed on a wafer substrate for XPS analysis, which was used to determine the binding energy between the ligand and the surface. The values of the binding energy were calibrated using the C1s peak, which was set at 284.6 eV.[44–48]

Computational details

We performed GGA-level spin-polarized Kohn–Sham DFT calculations with the atomic orbital-based $DMol^3$ software package.[49,50] The exchange-correlation energy was functionalized using the PW91 functional.[51,52] The Kohn–Sham equation was expanded in a double-numeric quality basis set with polarization functions. The orbital cutoff range was 5.0 Å. The DFT semicore pseudopotential[53] was used to treat the core electrons of the heavy Ag atoms. A Fermi smearing of 0.003 Ha (1 Ha = 27.2114 eV) was used in all calculations. The convergence tolerances of energy, force, and displacement were set at 2×10^{-5} Ha, 0.004 Ha $Å^{-1}$, and 0.005 Å, respectively.

To describe the surface of the 12.2 nm Ag NPs, we used an Ag (211) surface with 8 atomic layers (approximately 5.8 Å), a vacuum thickness of 20 Å, and a (2×4) supercell because the size of the Ag NPs in this study was approximately 12 nm. The atomic positions in all layers were allowed to relax during the geometry optimization and ligand adsorption calculation. The energy was calculated only at the Γ-point because of the large size of the supercell.

We adsorbed ligands such as methylamine (CH_3NH_2) and acetate ion (CH_3COO^-) to many adsorption sites on the Ag (211) surface to verify the ligand exchange reaction. In practice, ligands with long alkyl chains (such as OA) are used to synthesize Ag NPs. However, in this study, we considered the shortest alkyl chain (methyl [–CH_3]) as an equivalent to an OA to limit the computational cost.[54] In the case of the acetate ion, we used the acetate ion as is. For reliable results, we considered the net charge of the total system[55] by inserting or removing an electron from the total system because the net charge is altered by ligand adsorption during the chemical reaction. We addressed almost every possible condition to find strong adsorption sites and calculated the adsorption energy of the ligand (E_{ad}) given by following equation:[56–58]

$$E_{ad} = E_{Ag+lig} - E_{Ag} - E_{lig} \quad (1)$$

here, in eqn (1), E_{Ag+lig} is the total energy of the system where the ligand is adsorbed on the Ag surface, E_{Ag} is the total energy of the bare Ag (211) surface, and E_{lig} is the energy of the each ligand.

Results and discussion

Electrical properties and low-temperature processability

OA-capped 12.2 nm Ag NPs were satisfactorily synthesized by the procedure reported in our previous study.[30] Generally, it is

well known that electrical properties are closely related to the removal of the ligand shell because the curing temperature is defined as the temperature where particles lose their ligand shell and elicit conductance through physical contact with each other.[28,29,59] According to our previous study, approximately 12 wt% OA remained on the Ag NPs, although the residual OA was reduced by the methanol dipping treatment.[30] Mazumder and Sun have reported the use of a 10 h AA immersion treatment to remove OA from the NPs.[40] Therefore, we conducted an AA immersion treatment to enhance the electrical properties by additionally reducing the organic ligand layer. Fig. 1 shows the TGA results for the residual ligand at the surface with different AA immersion times. For samples that underwent the AA immersion treatment, the residual ligand was reduced with increasing immersion time: 4.49 wt% when immersed for 1 h, 4.23 wt% when immersed for 2 h, 3.89 wt% when immersed for 3 h, 3.11 wt% when immersed for 5 h and 2.36 wt% when immersed for 10 h. Thus, when the Ag NPs were immersed in AA, the capping ligand was dramatically reduced by approximately 10 wt% after 10 h and approximately 8 wt% even after only 1 h.

Recently, the percolation transformation has received attention as a possible means of curing metal NPs.[20,28,29] According to this concept, full melting and solidification are not required. Rather, the continuous structure and electrical properties can be found at a much lower temperature than the melting temperature because of the elimination of the ligand shells surrounding the metal NPs and the subsequent agglomeration induced by the physical contact and coalescence of the NPs.[8,30] According to the theory behind the percolation transformation, the reduction of the ligand layer is important for the agglomeration of NPs, which creates conductive paths or patterns. Thus, we could expect that the reduced ligand layer would elicit superior electrical performance from the TGA results. To investigate the electrical properties, we fabricated conductive ink with 30 wt% of Ag NPs, and the resistivity of the ligand-reduced Ag ink was compared with the resistivity of the OA-capped Ag ink, which was 5.63 μΩ cm at 250 °C for 20 min.[30] For the ligand-reduced Ag ink, as shown in Fig. 2(a), a similar resistivity (7.13 μΩ cm) was achieved at 250 °C for only 5 min, and less than 4.54 μΩ cm was achieved for more than 10 min of curing time. This value is close to the value for the bulk Ag (1.59 μΩ cm)[29] and better than the value for the OA-capped ink with the same conditions. In addition, the ligand-reduced Ag ink offered low-temperature-processability. In contrast to the OA-capped Ag ink, the ligand-reduced Ag ink showed excellent electrical properties at 200 °C, and resistivity of less than 10 μΩ cm was achieved at 100 °C and 150 °C with 1 h of curing time. It is important that 100 and 150 °C are sufficiently low temperatures to permit the use of plastic substrates for printed electronics. Fig. 2(b)–(d) shows the well-agglomerated surface morphology of the conductive film cured at 100 °C for 30 min, 1 h and 2 h. All values of resistivity were calculated by sheet resistance and measured thickness of the conductive films (200 ± 10 nm). According to the percolation transformation concept, such outstanding electrical performance is derived from the lower number of ligand shells produced by the AA immersion treatment, which makes it easy to remove the ligands and agglomerate the Ag NPs in the curing process. Furthermore, the AA immersion treatment results in not only a reduction but also an exchange of ligands, as discussed below. The thermally stable OA, which has a higher boiling point (approximately 350 °C), was exchanged with the acetate ion, which is a less stable ion with a shorter chain than OA. Therefore, we can expect the thermal elimination of the ligand to occur easily in the ligand-reduced and ligand-exchanged Ag NPs. Thus, ligand exchange as a result of AA immersion treatment can reduce the curing time and temperature. The electrical properties are dramatically improved and acceptable for application on plastic substrates.

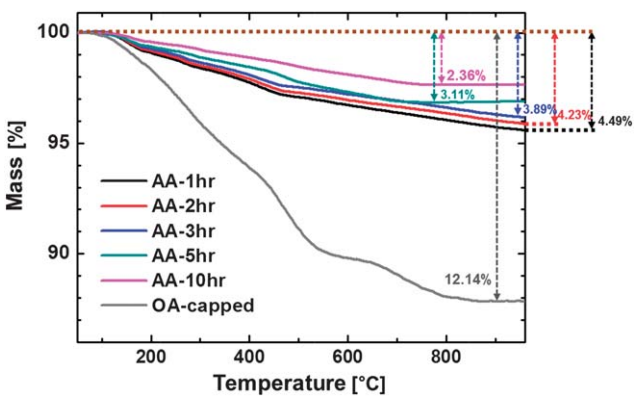

Fig. 1 TGA results for OA-capped Ag NPs and ligand-reduced Ag NPs after AA immersion treatments conducted for different durations. The weight loss was 4.49% for 1 h, 4.23% for 2 h, 3.89% for 3 h, 3.11% for 5 h and 2.36% for 10 h.

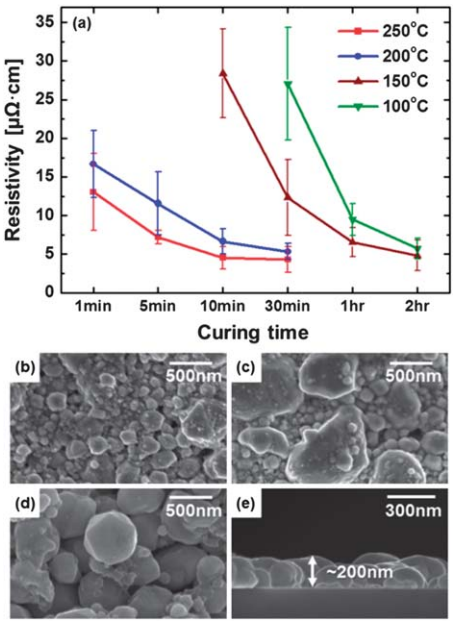

Fig. 2 (a) Electrical resistivity of the conductive Ag ink as a function of curing time and temperature. Surface morphology of conductive Ag ink cured at 100 °C for (b) 30 min, (c) 1 h and (d) 2 h. (e) Vertical section of the conductive film cured at 100 °C for 2 h.

To further investigate the particle agglomeration process, as shown in Fig. 3, *in situ* TEM was used to observe the ligand-dependent growth of individual particles with increasing temperature. Fig. 3(a)–(f) shows the behavior of the ligand-reduced Ag NPs with increasing temperature. Although the 12.2 nm particles were arranged well at room temperature, agglomeration began at 100 °C, as shown in Fig. 3(b), and the agglomerations grew larger with increasing temperature. In contrast, OA-capped Ag NPs that were not immersed in AA are shown in Fig. 3(g)–(l). The NPs were barely in contact below 150 °C and showed low agglomeration at 200 °C, as shown in Fig. 3(j). These results are almost in agreement with our previous results, in which curing at 150 °C almost produced an insulator effect, and electrical contact was observed at 200 °C.[30] Compared with the OA-capped Ag NPs, the ligand-reduced Ag NPs began to agglomerate at a much lower temperature (approximately 100 °C). Thus, ligand-reduced Ag NPs can form conductive pathways even at 100 °C.

Chemiadsorption of the ligand on the Ag NPs

Although the organic capping ligand on the surface was reduced and the electrical properties were enhanced by the AA immersion treatment, the surface chemistry was not identified by the surface analysis. Therefore, FTIR spectra were used to characterize the surface chemistry of the OA-capped (as-synthesized) and ligand-reduced (AA immersion processed) Ag NPs. Fig. 4(a) shows the typical FTIR spectra of pure OA and of OA-capped Ag NPs. The spectrum of the OA-capped Ag NPs is similar to the OA spectrum. In both curves, two sharp peaks at 2921 and 2852 cm^{-1} were attributed to the characteristics of the asymmetric and symmetric CH_2 stretching modes, respectively. The peak at 2952 cm^{-1} represented the C–H stretching mode of the OA carbon chain, and the bands at 1330–1650 cm^{-1} were attributed to the $-NH_2$ bending mode.[60,61] The surfactant ligands in the adsorbed state were strongly combined with the surface of the Ag NPs. As a result, the characteristic bands were shifted to a lower-frequency region by the deformation vibration of the primary amine.[62,63]

The FTIR spectra of pure AA and ligand-reduced Ag NPs are shown in Fig. 4(b). There were no peaks related to AA in the ligand-reduced Ag NPs, even though they were immersed in AA for 10 h. In AA, the intense peak at 1710 cm^{-1} originated from the C=O stretching mode, and the band at 1263 cm^{-1} was attributed to the C–O stretching mode.[63–65] In the case of the ligand-reduced Ag NPs, the characteristic stretching frequencies indicated the symmetric and asymmetric stretching modes of the carboxylate ion (COO^-) at 1405 and 1562 cm^{-1}, respectively.[62,66] Based on our findings and previous studies of carboxylates, the interaction between the carboxylate ion and the metal atom was categorized as three types: unidentate, bridging bidentate and chelating bidentate.[67–69] The wavenumber separation, Δ, between the $\nu_{as}(COO^-)$ and $\nu_s(COO^-)$ FTIR bands, can be used to distinguish the type of the interaction between the carboxylate head and the metal atom. The highest Δ (200–320 cm^{-1}) corresponded to the unidentate interaction, and the lowest Δ (below 110 cm^{-1}) was for the chelating bidentate interaction. The medium range of Δ (140–190 cm^{-1}) was for the bridging bidentate interaction. In this study, the Δ (1562 − 1405 = 157 cm^{-1}) was attributed to the bridging bidentate, which is consistent with the following results of the DFT calculation.

To further investigate the variation in the chemical structure of the Ag NPs using the AA immersion treatment, we determined the high-resolution XPS spectra of C1s. In the case of the OA-capped Ag NPs, as shown in Fig. 5(a), two C1s peaks were observed at 284.6 and 286.7 eV. Generally, the main peak at 284.6 eV is attributed to the carbon atoms in the alkane chain (C–C), and the peak at 286.7 eV is assigned to the superposition

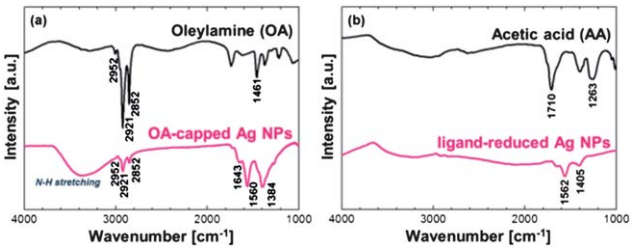

Fig. 4 FTIR spectra for (a) OA-capped Ag NPs and pure solvent and (b) ligand-reduced Ag NPs and pure AA.

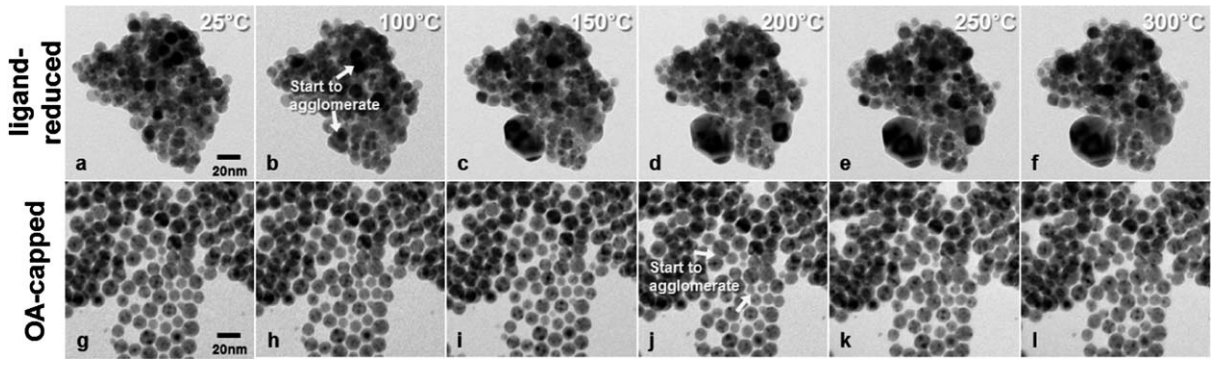

Fig. 3 *In situ* TEM results for Ag NPs capped with different ligands: (a)–(f) ligand-reduced Ag NPs, (g)–(l) original OA-capped Ag NPs, shown at increasing temperatures from 25 °C to 300 °C. In the case of ligand-reduced Ag NPs, agglomeration began at (b) 100 °C, in contrast to the OA-capped Ag NPs, where agglomeration began at (j) 200 °C.

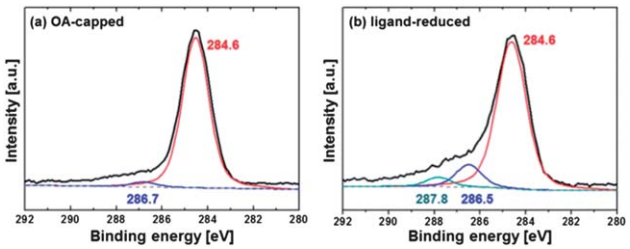

Fig. 5 XPS spectra of the C1s subregion for (a) OA-capped Ag NPs and (b) ligand-reduced Ag NPs. The measured spectra are represented by black lines, and the simulated individual peaks are indicated by colored lines. For clarification, an offset has been added to the simulated curves to permit comparison with the measured curves.

of different contributions (C–N and C–O).[70] There were some differences in the ligand-reduced Ag NPs. As shown in Fig. 5(b), we were able to fit three types of peaks in the curve. The peaks at 284.6 eV and 286.5 eV were similar to those for the OA-capped NPs; however, the other peak observed at 287.6 eV belonged to the carboxylate ($-COO^-$) carbon.[25,63,71] The C1s peak corresponded to carboxylic carbon (–COOH), located at 290.0 eV, which did not appear in the spectrum.[72] Both surface analyses helped to identify the ligand exchange from OA to the carboxylate ($-COO^-$) ion. Furthermore, we expect the carboxylate ion on the Ag NPs to be the acetate ion (CH_3COO^-) because it can be generated by the ionization of AA. Therefore, it is likely that ligand exchange was successfully achieved by the AA immersion treatment.

Adsorption energy of the ligand

As mentioned previously, we performed DFT calculations to evaluate the ligand exchange reaction on the surface of the Ag NPs. Thus, we calculated the adsorption energy of methylamine and acetate ions following a simple scheme to describe the ligand exchange reaction.

In Scheme 1, six simple states in the ligand modification reaction are shown, and they are composed of ligand adsorption and desorption. Through the process, the methylamine is being adsorbed on the surface of Ag NPs (1st and 2nd pictures of Scheme 1) because the amine was identified by surface chemistry analyses in Fig. 4 and 5. The surface chemistry also confirmed that only the acetate ions remained on the surface of Ag NPs (6th picture of Scheme 1) after the AA immersion treatment. Generally, the acetate ion (CH_3COO^-) can be generated by ionization of AA in an aqueous solution. And thus, we assumed the co-adsorbed state with amine and acetate ions (4th picture of Scheme 1) as an intermediate state because it was hard to find the other molecules or byproducts by means of experimental analyses. The 3rd and 5th pictures in Scheme 1 describe the adsorption of acetate ion and desorption of amine for better understanding of intermediate and final states, respectively. Although this scheme is oversimplified, we can suggest the reason for the ligand exchange reaction because the DFT calculation is based on the experimental results described above. Before we calculate the adsorption energy of the ligand following this scheme, we have to verify which adsorption site is the most stable site for each ligand and consider the charge transition in the whole system arising from the ligand adsorption on the Ag NPs.

Firstly, we address the adsorption site of each ligand. There were many possible adsorption sites when the methylamine and acetate ions were adsorbed on the Ag NP surface, so we considered almost every adsorption site to obtain reliable results. As shown in Scheme 2, there are five stable adsorption sites, as follows: t_1 (top site on the edge), t_2 (top site on the face), b_1 (bridge site on the edge), b_2 (bridge site on the face) and b_3 (bridge site between the edge and face). In these stable adsorption sites, the t_1 and t_2 sites belong to methylamine, and the b_1, b_2 and b_3 sites belong to the acetate ion. We calculated 7 to 9 adsorption sites for each ligand to verify their stability, but all of the adsorbed methylamines were eventually drawn to the top (t_1 or t_2) sites; in particular, t_1 was the strongest adsorption site, −0.587 eV.[54] Similarly, acetate ions were drawn to the bridge (b_1, b_2 or b_3) sites even though they were initially attached on the top site. These results are consistent with the experimental FTIR analysis, which indicated that the carboxylate ion in this study was in the bridging bidentate mode and not the unidentate or chelating bidentate modes.[67–69] The bridging bidentate mode is equivalent to adsorption at a bridge site in the DFT calculation. For the acetate ion, the b_1 site was the strongest adsorption site (−2.566 eV) among the three types of bridge sites. The adsorption energy of the acetate ion is four times stronger than that of amine. Then, an edge site is more

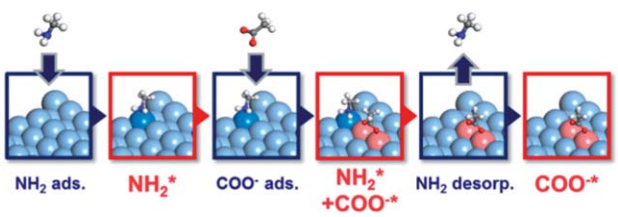

Scheme 1 The simple reaction scheme for the adsorption and desorption of the ligand (methylamine and acetate ion) throughout the process. The asterisk (*) on the right side represents the adsorbed ligand on the Ag NPs.

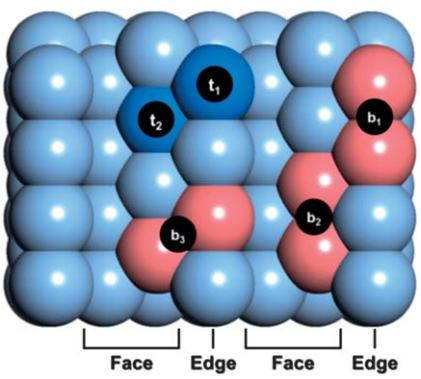

Scheme 2 The most stable site of each ligand: t_1 and t_2 are adsorption sites for methylamine; b_1, b_2 and b_3 are adsorption sites for acetate ion (t_1: top site on the edge, t_2: top site on the face, b_1: bridge site on the edge, b_2: bridge site on the face, b_3: bridge site between the edge and the face).

stable than a face site for both methylamine and acetate ions. Accordingly, the edge site on the surface of the Ag NPs is more active in the ligand adsorption than the face site because the edge site has many dangling bonding sites that can be affected by adsorption strength.[54] The Mulliken charge of the ligand represents the amount of charge transfer during the ligand adsorption, so a large amount of charge transfer means a strong interaction between Ag and the ligand. As shown in Table 1, the amount of charge transfer in acetate ion adsorption was about four times larger than that in amine adsorption. Therefore, the charge transfer was strongly related to adsorption energy of the ligand. The co-adsorbed intermediate state with amine and acetate ions is also represented in Table 1. In the case of the ligand co-adsorbed state, the amount of charge transfer with amine was similar or slightly reduced in comparison with the adsorption of amine alone, while that with acetate ions was similar or slightly increased. In other words, adsorption of acetate ions weakens the binding of amine from Ag NPs. Finally, the weakly bound amines are easily desorbed and only the acetate ions remain on the surface of Ag NPs.

The whole reaction procedure is shown in Fig. 6 which is drawn based on Table 1, and the red line in each stage refers to adsorption on the most stable edge sites. In contrast to Scheme 1, the reaction in Fig. 6 has a small difference in charge transition by ligand adsorption and desorption. Firstly, the amine is adsorbed on the neutral Ag NPs during the chemical synthesis. There are two states corresponding to t_1 and t_2 sites. The acetate ion is then adsorbed on the neutral Ag NPs and converts the net charge of the total system to negative, and these states correspond to six co-adsorbed sites: t_1-b_1, t_1-b_2, t_1-b_3, t_2-b_1, t_2-b_2 and t_2-b_3. Thus, we carefully considered the net charge of the system during all the DFT calculations in this study. In the three-step reaction in Fig. 6, the first step corresponds to the chemical synthesis of the Ag NPs and the remaining two steps take place in the AA immersion treatment. These two steps represent acetate ion adsorption followed by methyl amine desorption, so the acetate ions remain alone (b_1, b_2, and b_3 sites) on the surface of Ag NPs. Here, the relative energy difference between the state of methylamine being adsorbed and the state of acetate ion being adsorbed is approximately −1.98 eV. Thus, acetate ion adsorption is energetically much more favourable than the methylamine adsorption. Though the amine desorption process increases the relative energy, it can take place because it occurs at room temperature (approximately 300 K). In addition, adsorption of acetate ions weakens the binding of amine followed by reduced charge transfer, and thus the amine desorption becomes easy. Therefore, the ligand exchange reaction from amine to acetate ion occurs spontaneously because of the stability of the NPs with a large energy difference.

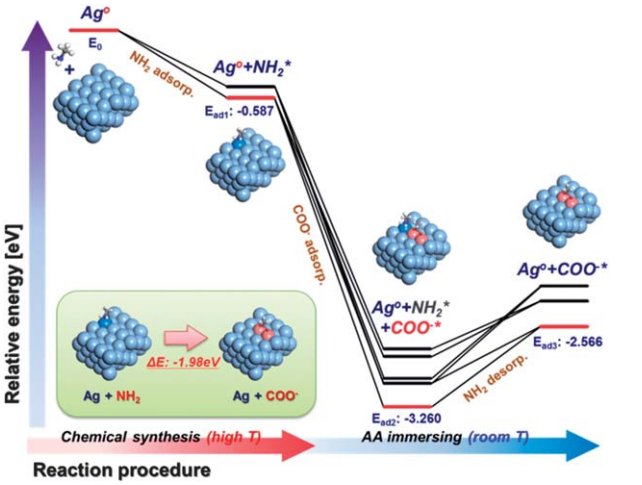

Fig. 6 The relative energy diagram along the reaction procedure (adsorption and desorption of the ligand on the Ag NPs). After NH_2 was adsorbed on the Ag NPs (chemical synthesis), the adsorption energy was increased by 1.98 eV upon ligand exchange (AA immersion treatment), *i.e.*, the adsorption of COO^- and desorption of NH_2 from the Ag NPs. The asterisk (*) on the right side represents the adsorbed ligand on the Ag NPs.

Table 1 The stable adsorption site, adsorption energy and the Mulliken charge of each ligand adsorption. Amine has two stable adsorption sites, and the acetate ion has three stable adsorption sites. There are six intermediate adsorption states because six combinations are possible with two stable amine sites and three acetate ion sites. The Mulliken charge of the ligand represents the amount of partial charge change in the ligand during the adsorption procedure

System	Site	E_{ad} [eV]	Amount of Mulliken charge
Amine	t_1	−0.587	0.157
	t_2	−0.490	0.156
Acetate ion	b_1	−2.566	0.505
	b_2	−2.346	0.503
	b_3	−2.214	0.495

System	Site	E_{ad} [eV]	Amount of Mulliken charge	
			Amine	Acetate ion
Amine + acetate ion	t_1-b_1	−3.260	0.137	0.535
	t_1-b_2	−2.825	0.157	0.524
	t_1-b_3	−3.016	0.134	0.490
	t_2-b_1	−3.058	0.154	0.606
	t_2-b_2	−2.758	0.158	0.524
	t_2-b_3	−2.929	0.125	0.496

Conclusions

Ligand-reduced Ag NPs were successfully obtained by a simple AA immersion treatment. In the case of ligand-reduced Ag NPs, superior electrical performance was observed even at low temperatures (100–150 °C) because of the reduction by 10 wt% of the residual OA, which was thermally stable. Experimentally, the AA immersion treatment resulted in not only ligand reduction but also ligand exchange from OA to the acetate ion, as indicated by FTIR and XPS analyses. The ligand exchange was explained by the difference in adsorption energy of the two ligands, as estimated by the DFT calculation. We have thus effectively overcome the drawback of conductive Ag ink related to its higher curing temperature, which is essential to permit its use on plastic substrates. Therefore, our process is a simple chemical treatment that can be used to create conductive Ag ink for printed electronics.

Acknowledgements

This research was supported by the NLRL (National Leading Research Laboratory) program through the National Research Foundation of Korea (NRF) grant funded by the Korea government (MEST) (no. 2011-0028612). An additional grant from the WCU (World Class University) program through the NRF of Korea MEST (no. R32-10051) is also acknowledged.

Notes and references

1 M. Singh, H. M. Haverinen, P. Dhagat and G. E. Jabbour, *Adv. Mater.*, 2010, **22**, 673.
2 B. J. De Gans, P. C. Duineveld and U. S. Schubert, *Adv. Mater.*, 2004, **16**, 203.
3 S. H. Ko, H. Pan, C. P. Grigoropoulos, C. K. Luscombe, J. M. J. Frechet and D. Poulikakos, *Nanotechnology*, 2007, **18**, 345202.
4 J. Park, D. J. Lee, S. J. Kim and J. H. Oh, *J. Micromech. Microeng.*, 2009, **19**, 095021.
5 C. N. Hoth, S. A. Choulis, P. Schilinsky and C. J. Brabec, *Adv. Mater.*, 2007, **19**, 3973.
6 V. Shrotriya, *Nat. Photonics*, 2009, **3**, 447.
7 M. Hilder, B. Winther-Jensen and N. B. Clark, *J. Power Sources*, 2009, **194**, 1135.
8 S. Sivaramakrishnan, B. T. Anto and P. K. H. Ho, *Appl. Phys. Lett.*, 2009, **94**, 091909.
9 K. T. Braam, S. K. Volkman and V. Subramanian, *J. Power Sources*, 2012, **199**, 367.
10 S.-C. Chang, J. Liu, J. Bharathan, Y. Yang, J. Onohara and J. Kido, *Adv. Mater.*, 1999, **11**, 734.
11 A. A. Argun, P.-H. Aubert, B. C. Thompson, I. Schwendeman, C. L. Gaupp, J. Hwang, N. J. Pinto, D. B. Tanner, A. G. MacDiarmid and J. R. Reynolds, *Chem. Mater.*, 2004, **16**, 4401.
12 A. Nathan and B. R. Chalamala, *Proc. IEEE*, 2005, **93**, 1235.
13 K. Song, D. Kim, X.-S. Li, T. Jun, Y. Jeong and J. Moon, *J. Mater. Chem.*, 2009, **19**, 8881.
14 T. Sekitani, H. Nakajima, H. Maeda, T. Fukushima, T. Aida, K. Hata and T. Someya, *Nat. Mater.*, 2009, **8**, 494.
15 J. B. Chang, V. Liu, V. Subramanian, K. Sivula, C. Luscombe, A. Murphy, J. Liu and J. M. J. Frechet, *J. Appl. Phys.*, 2006, **100**, 014506.
16 V. Subramanian, J. M. J. Frechet, P. C. Chang, D. C. Huang, J. B. Lee, S. E. Molesa, A. R. Murphy, D. R. Redinger and S. K. Volkman, *Proc. IEEE*, 2005, **93**, 1330.
17 P. Calvert, *Chem. Mater.*, 2001, **13**, 3299.
18 Y. H. Jo, I. Jung, N. R. Kim and H. M. Lee, *J. Nanopart. Res.*, 2012, **14**, 1.
19 Y. H. Jo, J. C. Park, J. U. Bang, H. Song and H. M. Lee, *J. Nanosci. Nanotechnol.*, 2011, **11**, 1037.
20 S. Sivaramakrishnan, P. J. Chia, Y. C. Yeo, L. L. Chua and P. K. H. Ho, *Nat. Mater.*, 2007, **6**, 149.
21 L. Polavarapu, K. K. Manga, K. Yu, P. K. Ang, H. D. Cao, J. Balapanuru, K. P. Loh and Q.-H. Xu, *Nanoscale*, 2011, **3**, 2268.
22 R. S. Ingram, M. J. Hostetler and R. W. Murray, *J. Am. Chem. Soc.*, 1997, **119**, 9175.
23 M. J. Hostetler, S. J. Green, J. J. Stokes and R. W. Murray, *J. Am. Chem. Soc.*, 1996, **118**, 4212.
24 M. A. White, J. A. Johnson, J. T. Koberstein and N. J. Turro, *J. Am. Chem. Soc.*, 2006, **128**, 11356.
25 R. De Palma, S. Peeters, M. J. Van Bael, H. Van den Rul, K. Bonroy, W. Laureyn, J. Mullens, G. Borghs and G. Maes, *Chem. Mater.*, 2007, **19**, 1821.
26 Y.-M. Huh, Y.-W. Jun, H.-T. Song, S. Kim, J.-S. Choi, J.-H. Lee, S. Yoon, K.-S. Kim, J.-S. Shin, J.-S. Suh and J. Cheon, *J. Am. Chem. Soc.*, 2005, **127**, 12387.
27 R. Hong, N. O. Fischer, T. Emrick and V. M. Rotello, *Chem. Mater.*, 2005, **17**, 4617.
28 J. R. Greer and R. A. Street, *J. Appl. Phys.*, 2007, **101**, 103529.
29 J. Perelaer, A. W. M. de Laat, C. E. Hendriks and U. S. Schubert, *J. Mater. Chem.*, 2008, **18**, 3209.
30 I. Jung, Y. H. Jo, I. Kim and H. M. Lee, *J. Electron. Mater.*, 2012, **41**, 115.
31 D. Wakuda, M. Hatamura and K. Suganuma, *Chem. Phys. Lett.*, 2007, **441**, 305.
32 D. H. Kim, H. Y. Kim, H. G. Kim, J. H. Ryu and H. M. Lee, *J. Phys.: Condens. Matter*, 2008, **20**, 035208.
33 H. Y. Kim, H. G. Kim, D. H. Kim and H. M. Lee, *J. Phys. Chem. C*, 2008, **112**, 17138.
34 J. H. Ryu, D. H. Seo, D. H. Kim and H. M. Lee, *Phys. Chem. Chem. Phys.*, 2009, **11**, 503.
35 J. H. Ryu, H. Y. Kim, D. H. Kim, S. K. Choi and H. M. Lee, *J. Nanosci. Nanotechnol.*, 2009, **9**, 2553.
36 D. H. Kim, H. Y. Kim, J. H. Ryu and H. M. Lee, *Phys. Chem. Chem. Phys.*, 2009, **11**, 5079.
37 J. H. Ryu, H. Y. Kim, D. H. Kim, D. H. Seo and H. M. Lee, *J. Phys. Chem. C*, 2010, **114**, 2022.
38 D. Wakuda, K. S. Kim and K. Suganuma, *Scr. Mater.*, 2008, **59**, 649.
39 D. Wakuda, K. S. Kim and K. Suganuma, *IEEE Trans. Compon. Packag. Technol.*, 2009, **32**, 627.
40 V. Mazumder and S. Sun, *J. Am. Chem. Soc.*, 2009, **131**, 4588.
41 B. Hu, K. Ding, T. Wu, X. Zhou, H. Fan, T. Jiang, Q. Wang and B. Han, *Chem. Commun.*, 2010, **46**, 8552.
42 Y. H. Jo, I. Jung, C. S. Choi, I. Kim and H. M. Lee, *Nanotechnology*, 2011, **22**, 225701.
43 S. Yang, L. Wang, X. Tian, Z. Xu, W. Wang, X. Bai and E. Wang, *Adv. Mater.*, 2012, **24**, 4676.
44 C. Y. Tang, Y.-N. Kwon and J. O. Leckie, *J. Membr. Sci.*, 2007, **287**, 146.
45 J. Benavente and M. I. Vázquez, *J. Colloid Interface Sci.*, 2004, **273**, 547.
46 H. Pan, J. B. Yi, L. Shen, R. Q. Wu, J. H. Yang, J. Y. Lin, Y. P. Feng, J. Ding, L. H. Van and J. H. Yin, *Phys. Rev. Lett.*, 2007, **99**, 127201.
47 A. Radi, M. Ebrahimi and K. T. Leung, *Surf. Sci.*, 2010, **604**, 1073.
48 L. Meng, P. Wu, G. Chen and C. Cai, *J. Electrochem. Soc.*, 2008, **155**, F231.
49 B. Delley, *J. Chem. Phys.*, 2000, **113**, 7756.

50 B. Delley, *Comput. Mater. Sci.*, 2000, **17**, 122.
51 J. P. Perdew and Y. Wang, *Phys. Rev. B: Condens. Matter Mater. Phys.*, 1992, **45**, 13244.
52 J. P. Perdew, K. Burke and Y. Wang, *Phys. Rev. B: Condens. Matter Mater. Phys.*, 1996, **54**, 16533.
53 B. Delley, *Phys. Rev. B: Condens. Matter Mater. Phys.*, 2002, **66**, 155125.
54 J. H. Ryu, S. S. Han, D. H. Kim, G. Henkelman and H. M. Lee, *ACS Nano*, 2011, **5**, 8515.
55 D. H. Kim, K. Shin and H. M. Lee, *J. Phys. Chem. C*, 2011, **115**, 24771.
56 H. Y. Kim, S. S. Han, J. H. Ryu and H. M. Lee, *J. Phys. Chem. C*, 2010, **114**, 3156.
57 K. Shin, D. H. Kim, S. C. Yeo and H. M. Lee, *Catal. Today*, 2012, **185**, 94.
58 H. Y. Kim, H. M. Lee and G. Henkelman, *J. Am. Chem. Soc.*, 2011, **134**, 1560.
59 J. Perelaer, P. J. Smith, D. Mager, D. Soltman, S. K. Volkman, V. Subramanian, J. G. Korvink and U. S. Schubert, *J. Mater. Chem.*, 2010, **20**, 8446.
60 Z. Xu, C. Shen, Y. Hou, H. Gao and S. Sun, *Chem. Mater.*, 2009, **21**, 1778.
61 M. Salavati-Niasari, Z. Fereshteh and F. Davar, *Polyhedron*, 2009, **28**, 126.
62 J. Zhang and J. Fang, *J. Am. Chem. Soc.*, 2009, **131**, 18543.
63 L. Zhang, R. He and H.-C. Gu, *Appl. Surf. Sci.*, 2006, **253**, 2611.
64 J. P. I. de Souza, S. L. Queiroz, K. Bergamaski, E. R. Gonzalez and F. C. Nart, *J. Phys. Chem. B*, 2002, **106**, 9825.
65 D. Q. Vo, E.-J. Kim and S. Kim, *J. Colloid Interface Sci.*, 2009, **337**, 75.
66 L. J. Kirwan, P. D. Fawell and W. van Bronswijk, *Langmuir*, 2003, **19**, 5802.
67 K. Nakamoto, *Infrared and Raman Spectra of Inorganic and Coordination Compounds*, Wiley, New York, 1997.
68 Y. Ren, K.-I. Iimura and T. Kato, *Langmuir*, 2001, **17**, 2688.
69 J. Simon-Kutscher, A. Gericke and H. Hühnerfuss, *Langmuir*, 1996, **12**, 1027.
70 G. Dodero, L. De Michieli, O. Cavalleri, R. Rolandi, L. Oliveri, A. Daccà and R. Parodi, *Colloids Surf., A*, 2000, **175**, 121.
71 A. L. Willis, N. J. Turro and S. O'Brien, *Chem. Mater.*, 2005, **17**, 5970.
72 E. Frydman, H. Cohen, R. Maoz and J. Sagiv, *Langmuir*, 1997, **13**, 5089.

